Theoretical calculation and experiment of the impact characteristics in the plane ultrasonic rolling

Shuai-ling Lan (lanshuailing@163.com)
Kaifeng University
Meng Qi
Ming-xian Liu
Wen-bo Bie

Research Article

Keywords: plane ultrasonic rolling, impact characteristics, surface integrity, parameter optimization

Posted Date: May 31st, 2022

DOI: https://doi.org/10.21203/rs.3.rs-1625651/v1

Abstract

To achieve high machining efficiency in optimal surface integrity manufacturing, a relationship model between rolling depth and rolling force was established based on Hertz contact theory, and a theoretical model of impact characteristics was established according to the indentation geometry to evaluate the machining efficiency. Subsequently, the plane ultrasonic rolling experiment of 7075 aluminum alloy was carried out to verify the relationship between rolling depth and rolling force, meanwhile, the mapping between process parameters and surface characteristics, impact characteristics and surface morphology were studied, respectively. On this basis, the surface integrity prediction model was established by using nonlinear curve fitting method, and the optimal parameter solution was obtained by using quantum genetic algorithm (NSGA-□). The results show that the rolling force increases linearly with the increase in rolling depth. The impact characteristics increase with the increase in static force and amplitude, and decreases with the increase in step and feed rate, and the impact characteristics is negatively correlated with the processing efficiency. The optimization results provide a reference for engineering applications.

1. Introduction

The fatigue life of metallic components is determined largely by surface quality, such as surface roughness, micro-hardness and residual stress [1–3]. To date, compared with shot peening [4], laser intensification [5], and supersonic particle bombardment [6], the ultrasonic rolling processing (USRP) has been regarded as an outstanding technique to enhance material surface quality and maintain invariant the interior chemical composition of the material [7, 8]. It is mainly reflected in two aspects: one is to improve the surface characteristics, for example, Zhu [9], Bozdana [10], Cheng [11], Yang [12] research the effect of process parameters on surface integrity, and illustrated that better surface quality could be obtained at the static force, and bad influence would occur beyond a certain range. The other is to improve the fatigue life, for instance, Zhao [13], Liu [14] and ye [15] demonstrated that ultrasonic rolling leads to improved fatigue life, and can be of great help to improve the stability of materials.

From the above overview, many researchers [16–17] have investigated the influence of processing parameters on surface integrity. However, when optimal surface characteristic is obtained, the process parameters have been shown to be low spindle speed and slow feed rate, which affect to some extent workpiece processing efficiency. In order to alleviate the above problem, optimization and prediction of high processing efficiency and optimal surface characteristic are researched.

Firstly, the relationship between rolling depth and rolling force in planar ultrasonic rolling was established based on Hertz contact theory. Subsequently, according to the indentation geometry, the impact characteristic model is established to evaluate the machining efficiency. Then, the prediction model of surface integrity was established, and the optimal parameters of machining efficiency and surface performance were obtained.

2. Rolling Depth Model For In-plane Ultrasonic Rolling

During in-plane ultrasonic rolling, mechanical vibration of the roller is generated by an ultrasonic generator impulses from the static force and from the ultrasonic vibration are transferred to the workpiece surface by the roll, as is shown in Fig. 1.

Based on the mechanism of ultrasonic rolling, the workpiece surfaces will undergo elastic-plastic deformation as the roller comes into contact with the workpiece. According to Hertz contact theory, an indentation is formed whose depth is as same as the sum of the reduction and the amplitude of the applied vibration. When the roller is removed, the depth of the indentation decreases because of the elastic recovery, as is shown in Fig. 2.

According to relevant geometric relations, Eq. (1) can be obtained:

$$h_a = h_0 + A_0 - h_e$$

1

Where, h_a, h_0, A_0, and h_e are actual depth, nominal depth, amplitude and magnitude of elastic recovery, respectively.

The unloading process can be assumed to be an elastic process because the reduction is not too large. Based on the elastic half-space volume, the magnitude of elastic recovery is expressed in the Eq. (2).

$$h_e = \sqrt{\frac{9\pi}{16}\frac{FHv}{E^{*2}}}$$

2

Where, $E^*=E_1/(1-\mu_1)+E_2/(1-\mu_2)$, E_1 and E_2 are the elastic modulus of the roller and the plane, respectively. μ_1 and μ_2 are the Poisson ratios of the roller and the plane, respectively, F is the rolling force, and Hv is the workpiece surface micro-hardness.

Therefore, the relationship between the rolling force and the nominal rolling depth should be established to obtain the actual rolling depth.

3 Mechanical Analysis Of Plane Ultrasonic Rolling

When the roller comes into contact with the workpiece, the workpiece surfaces will undergo the elastoplastic deformation. However, compared with the plastic deformation, the elastic deformation is smaller and will rebound after application of USRP. Therefore, the displacement of elastic recovery is ignored and only the plastic deformation is analyzed. The specific force analysis is shown in Fig. 3.

Where, F is the static force; N is the pressure exerted by the workpiece on the roller; f is the friction force exerted by the workpiece on the roller; R_T is the radius of the roller; θ and $\varnothing$ are the contact angle in the x-z

plane and in the x-y plane, respectively. According to the Hertz contact theory, the contact shape is an approximately spherical cap [18]. In order to obtain the N acting on the roller in the contact zone, the contact area is divided into j discrete equally spaced units. The area of each interval is very small, so the N_i is assumed to be approximately constant: dN in the i^{th} interval. The N acting on the roller can be calculated by integrating over the contact zone:

$$\vec{N} = \iint \overrightarrow{dN}$$

3

Where, $dN = P_m dA = P_m(R_T d\theta)(R_T \sin\theta d\varphi) = P_m R_T^2 \sin\theta d\theta d\varphi$, P_m is the average surface stress in the contact zone. Then, the N is distributed along the axes:

$$\vec{N} = \vec{N}_x + \vec{N}_y + \vec{N}_z$$

4

$$\vec{N}_x = -\iint dN \sin\theta \sin\phi = -P_m R_T^2 \int_0^{\theta} \sin^2\alpha d\alpha \int_0^{\pi} \sin\phi d\phi$$

5

$$\vec{N}_y = -\iint dN \cos\theta = -P_m R_T^2 \int_0^{\theta} \sin\alpha\cos\alpha d\alpha \int_0^{\pi} d\phi$$

6

$$\vec{N}_z = 0$$

7

Where, the minus sign means that $\vec{N}_x$ and $\vec{N}_y$ are opposite to the x-axis and y-axis, respectively.

According to Coulomb's law, the forces of friction along the axis are calculated as follows.

$$\vec{f} = \iint \overrightarrow{df}$$

8

$$\vec{f} = \vec{f}_x + \vec{f}_y$$

9

$$\vec{f}_x = \mu\vec{N}_y = -\mu P_m R_T^2 \int_0^{\theta} \sin\alpha\cos\alpha d\alpha \int_0^{\pi} d\phi \quad (10)$$

$$\vec{f}_y = \mu\vec{N}_x = -\mu P_m R_T^2 \int_0^{\theta} \sin^2\alpha d\alpha \int_0^{\pi} \sin\phi d\phi$$

11

Where, $d\vec{f}$ and $d\vec{N}$ are perpendicular, and μ is the friction coefficient between the roller and the workpiece.

According to the relationship of the Newtonian law, the forces acting on the roller are balanced in USRP, so the net force along the *y*-axis is zero:

$$\vec{F} + \vec{N}_y + \vec{f}_y = 0$$

12

Substituting Eq. (6) and Eq. (11) into Eq. (12):

$$F = \frac{1}{4}\pi R_T^2 P_m \left[(1 - \cos 2\alpha) - \frac{2}{\pi}\mu(2\alpha - \sin 2\alpha) \right] \approx \pi R_T P_m h_a \left[1 - \mu\sqrt{\frac{h_0}{2R_T}} \right]$$

13

Because h_a is much less than $2R_T$, is approximated to 0. μ is very small, and P_m is approximately set as the workpiece surface micro-hardness Hv, then the Eq. (13) is simplified as follows:

$$F = \pi R_T P_m h_a = \pi R_T H v h_a$$

14

It can be seen from the Eq. (14) that there is a linear relationship between the rolling depth and the rolling force.

4. The Impact Characteristics Between Workpiece And Roller

4.1 The geometric contact model of ultrasonic rolling

The geometric contact model between the roller and the workpiece is shown in Fig. 4. According to the relevant mathematical relations, Eq. (15) can be obtained:

$$R_T^2 = a^2 + (R_T - h_a)^2$$

15

Considering that h_a^2 is a high-order infinitesimal, Eq. (15) can be simplified to Eq. (16):

$$a = \sqrt{2R_T h_a}$$

16

4.2 The model of the impact characteristics

As is shown in Fig. 5a, the actual contact trajectory K between the roller and the workpiece is a sine curve in the USRP. As is shown in Fig. 5b, L and *b* are the step and the processing length, respectively. The processing area S_C = L×b, the actual impact area S_U = 2a×K. The impact characteristic *W*, identified as the number of shocks per unit area, is expressed in Eq. (17):

$$W = \frac{2a \cdot K}{L \cdot b} = \frac{\sqrt{8R_T h_a}\int_0^{\frac{b}{v}} \sqrt{1 + (2\pi f A_0)^2 \cos^2(2\pi f t)}\, dt}{Lb}$$

17

When the rolling force decreases, the step increases, and the feed speed increases. It is possible to cause *W* to be less than 1, which leads to intermittent processing. In contrast, when *W* is larger than 1, the unit area acting on the workpiece surface was subject to *W* (> 1) shock. It is not hard to see that the more significant the impact characteristics, the lower the machining efficiency. In other words, it is necessary to pursue the lowest impact number and achieve the optimal surface quality.

5. The Platform Of Ultrasonic Rolling

The ultrasonic rolling experiments were carried out on vertical machining center, type VMC-850E. The experimental system was composed of a Kistler dynamometer (9257b) and a bespoke wireless transmission ultrasonic vibration-assisted rolling system, as is shown in Fig. 6.

The material of the roller was YG8 cemented carbide, and the reinforced material was 7075 aluminum alloy with a Vickers hardness of 325Hv. Their mechanical properties are shown in Table 1.

Table 1
Mechanical Performance Parameters of the Material

Material	Density/(kg.m^{-3})	Modulus/GPa	Poisson Ratio /μ	Tangent Modulus/MPa	Yield Stress/MPa
YG8	14500	600	0.21	/	/
7075	2600	70	0.3	300	450

After the USRP, the residual stress σ, surface roughness Ra, surface hardness Hv are measured by the PROTO X-ray unit, Taylor Hobson rough meter (Subtonic 3+), and micro-hardness instrument (MH-5), respectively. In particular, a Cu target and the force of 30N last for 10 second are accepted in the measurements of residual stress and hardness, respectively.

6 Results And Analysis

The corresponding test parameters and test plan are shown in Tables 2 and 3, respectively.

Table 2
Experiment Parameters

Item	parameter
n/r.min^{-1}	3000
v/mm.min^{-1}	60, 80, 100, 120
F/mm	120, 180, 240, 300
L/mm	0.05, 0.1, 0.15, 0.2
R_T/mm	3
f/KHz	30
A_0/μm	2, 2.5, 3, 3.5

Table 3
Test scheme and results

No	Static force	Feed Rate	Step	Amplitude	Results			impact characteristics
	F/N	*v*/r.min^{-1}	*L*/mm	A_0/μm	σ/MPa	H/Hv	Ra/μm	W/times
1	120	60	0.05	2	-251	528	0.47	24.8
2	120	80	0.1	2.5	-229	476	0.58	11.3
3	120	100	0.15	3	-218	432	0.61	7.0
4	120	120	0.2	3.5	-204	421	0.64	5.1
5	180	60	0.1	3	-345	554	0.48	30.8
6	180	80	0.05	3.5	-373	582	0.44	24.1
7	180	100	0.2	2	-255	478	0.58	3.9
8	180	120	0.15	2.5	-280	489	0.55	4.1
9	240	60	0.15	3.5	-417	597	0.47	29.9
10	240	80	0.2	3	-380	551	0.53	10.2
11	240	100	0.05	2.5	-409	632	0.40	10.9
12	240	120	0.1	2	-339	574	0.45	4.8
13	300	60	0.2	2.5	-452	611	0.49	19.8
14	300	80	0.15	2	-419	615	0.47	9.5
15	300	100	0.1	3.5	-481	638	0.44	12.7
16	300	120	0.05	3	-492	689	0.39	11.2

6.1 Relationship between rolling force and rolling depth

It can be seen from Fig. 7 that the rolling force increases linearly with the increase of the rolling depth, which is consistent with the conclusions in the literature [14, 21]. The values obtained from the experimental were smaller than the theoretical values, and the reason is that ultrasonic vibration usually can reduce the applied contact force. However, the discrepancy between the values was within 10%.

6.2 Influence of the parameters on the surface properties and the impact characteristics

The influence of the parameters on the surface properties and the impact characteristics is presented in Fig. 8. It can be observed that, on a whole, the residual compressive stress, surface hardness and the

impact times rise with the increase in the static force and amplitude. On the one hand, according to the literature [13, 22], the reason is that the plastic strain energy transmitted to the workpiece increases with the increase of static force and amplitude. On the other hand, according to Eqs. (14), (16) and (17), with the increase in the static force, the overlapping area of two adjacent indentations increases due to the contact radius increases, which gives rise to enhance the impact characteristics. That is to say, as the impact characteristics increases, the number of times of shock (from the ultrasonic pulses) increase per unit area. The times of shock are positively correlated with the residual compressive stress [23]. Therefore, the residual compressive stress can be increased effectively by increasing the static force.

With the increase of step and feed speed, the surface hardness, residual compressive stress and impact characteristics decrease significantly. The surface roughness is not sensitive to feed speed, but increases sharply with the increase of step. This is because the indentation area is greatly affected by the step. It is the decrease of the indentation area and the increase of the residual height that lead to the deterioration of the surface roughness. However, it is obvious that the processing efficiency has been improved.

6.2 Influence of impact characteristics on surface morphology

The influence of impact characteristics on surface morphology is shown in Fig. 9. It is seen from Fig. 9(a) to (d) that with the increase of impact times, the surface topography gradually tends to be flat, which is because the workpiece surface is repeatedly impacted and the superposition effect of peak-valley of materials is obviously improved. At the same time, the surface residual compressive stress and hardness are also greatly increased according to the experimental. However, better surface integrity is achieved at the expense of machining efficiency due to the reduction of step. It can be seen from Fig. 9(e) to (h) that although the difference of surface morphology is not obvious when the number of impact is constant, the surface integrity and machining efficiency are quite different. For example, the machining efficiency in Fig. 9(e) is about twice that in Fig. 9(h), but the residual compressive stress and surface hardness in Fig. 9(h) are about 1.5 times that in Fig. 9(e). This is due to the balance between rolling force and step. Therefore, the surface roughness deterioration caused by step can be improved by appropriately increasing rolling force. The surface morphologies under the two extremes of impact number are shown in Fig. 9 (I) and Fig. 9 (J), respectively. When the number of impacts is too large, although excellent residual compressive stress and hardness can be obtained, pits are generated due to repeated impacts on the workpiece per unit area, as shown in Fig. 9(I). On the contrary, when the impact number is too small, the phenomenon of intermittent processing is occurred due to the adjacent indentation area cannot be interfered.

In short, it can be seen from Fig. 9 that a larger residual compressive stress, hardness, and smaller surface roughness can be obtained by increasing appropriately the times of impact. But, it is bound to reduce processing efficiency. In order to obtain the process parameters that will give high efficiency and large residual compressive stress, hardness, and small surface roughness, the impact time is taken as a

method to evaluate the processing efficiency and to identify the optimal parameters. In other words, it is the ultimate goal that is to achieve both the minimum number of shocks and the optimal surface quality.

7 Multi-objective Optimization

7.1 The prediction of surface integrity and the impact characteristics

Based on the experimental results, the predictive model for surface integrity and the impact characteristics were established using the nonlinear regression method. By virtue of variance analysis and *F* tests, the regression Eq. (18) was demonstrated to be accurate at a confidence level of 96.3%, which shows the strong correlation between predicted values and measured values.

$$\begin{cases} \sigma = -197.4 - 1.3e^{-3}x_1^2 - 4.3e^{-3}x_2^2 - 2175x_3^2 - 9.1x_4^2 - 2e^{-3}x_1x_2 - 0.7x_1x_3 \\ \quad - 0.123x_1x_4 + 7.5x_2x_3 + 0.27x_2x_4 + 115x_3x_4 \\ H = 506.1 + 1.9e^{-3}x_1^2 + 6.9e^{-3}x_2^2 + 2882.4x_3^2 + 10.45x_4^2 + 2.6e^{-3}x_1x_2 - 2.15x_1x_3 \\ \quad + 0.03x_1x_4 - 7.25x_2x_3 - 0.6x_2x_4 - 56.1x_3x_4 \\ Ra = 0.5 - 1.1e^{-6}x_1^2 - 1.3e^{-5}x_2^2 - 2.13x_3^2 - 0.02x_4^2 - 2.7e^{-6}x_1x_2 + 1.7e^{-3}x_1x_3 \\ \quad - 2.6e^{-5}x_1x_4 + 7.3e^{-3}x_2x_3 + 9.8e^{-4}x_2x_4 + 0.115x_3x_4 \\ W = 28.9 + 3.6e^{-4}x_1^2 + 3.6e^{-3}x_2^2 + 319.2x_3^2 + 3.04x_4^2 - 2e^{-3}x_1x_2 - 0.65x_1x_3 \\ \quad + 0.034x_1x_4 - 0.1x_2x_3 - 0.23x_2x_4 - 7x_3x_4 \end{cases}$$

18

Where, x_1, x_2, x_3, x_4 representing the values of F, v, L, A0, respectively.

To verify the reliability of the prediction model, the predicted and test values were compared, as shown in Fig. 10. The maximum error are 6.6%. These results illustrate that the predicted value was close to test results. Therefore, the model was demonstrated to have a high prediction precision within the scope of the applied tests.

7.2 Multi-objective optimization results and discussion

NSGA-Ⅱ has been used in machining process because of fast non-dominated sorting approach, fast crowded distance estimation procedure, and simple crowded comparison operator among a lot of multi-objective optimization method. The mathematical equations and constraint conditions of optimization

procedure were established. First of all, construct optimization variables: $x=(x_1, x_2, x_3, x_4)$. Then, according to NSGA-Ⅱ and experiment design, constraint condition were constructed, as shown in Eqs. (19) to (22).

F: $120\text{N} \leq F \leq 300\text{N}$,

$$\left\{ \begin{array}{*{20}{c}} {{g_1}{\text{()}x{\text{()}}}=120 - {x_1} \leqslant 0} \\ {{g_2}{\text{()}x{\text{()}}}= {x_1} - 300 \leqslant 0} \end{array}} \right.$$
19

v: $60\text{r.min}^{-1} \leq v \leq 120\text{r.min}^{-1}$,

$$\left\{ \begin{array}{*{20}{c}} {{g_{\text{3}}}{\text{()}x{\text{()}}}={\text{6}}0 - {x_{\text{2}}} \leqslant 0} \\ {{g_{\text{4}}}{\text{()}x{\text{()}}}={x_{\text{2}}} - {\text{12}}0 \leqslant 0} \end{array}} \right.$$
20

L: $0.05\text{mm} \leq v \leq 0.2\text{mm}$,

$$\left\{ \begin{array}{*{20}{c}} {{g_{\text{5}}}{\text{()}x{\text{()}}}={\text{0}}{\text{.05}} - {x_{\text{3}}} \leqslant 0} \\ {{g_{\text{6}}}{\text{()}x{\text{()}}}={x_{\text{3}}} - {\text{0}}{\text{.2}} \leqslant 0\;\;} \end{array}} \right.$$
21

A_0: $2\mu\text{m} \leq v \leq 3.5\mu\text{m}$,

$$\left\{ \begin{array}{*{20}{c}} {{g_{\text{7}}}{\text{()}x{\text{()}}}={\text{0}}{\text{.05}} - {x_{\text{4}}} \leqslant 0} \\ {{g_{\text{8}}}{\text{()}x{\text{()}}}={x_{\text{4}}} - {\text{0}}{\text{.2}} \leqslant 0\;\;} \end{array}} \right.$$
22

In order to obtain better surface quality and higher processing efficiency, the multi-objective function considers optimization of residual stress, surface hardness, surface roughness and processing efficiency simultaneously. The optimization model is given in Eq. (23).

$$\left\{ \begin{array}{*{20}{c}} {{\text{Object: max}}}f{\text{(-\varvec{\sigma}()}x{\text(), H(x), -Ra(x), w()}x{\text())}}} \\ {{\text{Find:}}\;{x_1},{x_2},{x_3},{x_4}} \\ {{\text{s}}{\text{.t}}{\text{.}}{g_i}{\text{()}x{\text()}} \leqslant 0\;\;\;i=1,2,3 \cdots ,13.} \end{array}} \right.$$
23

Table 4
Pareto optimal solutions for optimization

F	v	L	A_0	σ	H	Ra	W
N	$mm \cdot min^{-1}$	mm	μm	Mpa	Hv	μm	/
228	112	0.12	3.3	-382	573	0.51	13.0
232	111	0.12	3.3	-386	578	0.48	13.8
237	109	0.11	3.3	-391	582	0.48	14.4
239	106	0.11	3.3	-399	589	0.46	15.2
241	104	0.11	3.3	-409	597	0.45	16.9
245	102	0.10	3.4	-413	603	0.44	17.5
248	100	0.10	3.4	-422	611	0.43	17.9
251	99	0.10	3.4	-430	619	0.42	18.1
256	98	0.10	3.4	-436	627	0.40	20.1
261	97	0.099	3.4	-460	633	0.37	20.7
265	95	0.099	3.4	-465	641	0.36	24.6
271	95	0.097	3.4	-471	650	0.34	24.9
276	94	0.095	3.4	-475	659	0.33	27.3

The optimal solution of surface quality is that the machining efficiency reaches the maximum when the maximum residual compressive stress, the highest surface hardness and the lowest surface roughness are satisfied. The partial optimal solution is given in Table 4, when the force is in the range of 228N to 276N, the feed speed is in the range of 94mm.min^{-1} to 112mm.min^{-1}, the step is in the range of 0.095mm to 0.12mm, and the amplitude is in the range of 3.3μm to 3.4μm, the outstanding surface integrity and machining efficiency can be achieved simultaneously.

8 Conclusions

(1) The rolling force increases linearly with the increase of rolling depth, and the experimental value is about 10% less than the theoretical value due to ultrasonic vibration.

(2) The residual compress stress, surface hardness increase with the increase in static force and amplitude, and decreases with the increase in step and feed speed. The surface roughness increases with

the increase of step and decreases with the increase of force and amplitude, and it is not sensitive to the feed speed.

(3) The impact number decrease as the rolling force decreases, the step increases, and the feed speed increases. When the number of impact is greater than 1 and less than 1, it is the criterion of intermittent and continuous machining, respectively. The impact characteristics is negatively correlated with the processing efficiency.

(4) The optimal parameters of the outstanding surface integrity and machining efficiency are in the range of 228N to 276N, the feed speed is in the range of 94mm.min^{-1} to 112mm.min^{-1}, the step is in the range of 0.095mm to 0.12mm, and the amplitude is in the range of 3.3μm to 3.4μm.

Declarations

Funding

This research was supported by the Key R&D and Promotion Program (Science and Technology) in Henan Province, China (No.222102220003).

Conflicts of interest

The authors declare that no potential conflicts of interest with respect to the research, authorship, and/or publication of this article.

Availability of data and materials

The datasets used or analyzed during the current study are available from the corresponding author on reasonable request.

Ethical Approval

The authors state that this paper is an original work, it has not been published in any journals, and this research does not involve any ethical issues of humans or animals.

Consent to Participate

The authors declare that this research involves no Human Participants and/or Animals.

Consent to Publishcation

The authors confirm:

the paper described has not been published before,

that it is not under consideration for publication elsewhere,

that its publication has been approved by all co-authors,

that its publication has been approved by the responsible authorities at the institution where the work is carried out.

The authors agree to publication in the Journal indicated below and also to publication of the article in English by Springer in springer's corresponding English-language journal.

The copyright to the English-language article is transferred to Springer effective if and when the article is accepted for publication. The author warrants that his/her contribution is original and that he/she has full power to make this grant. The author signs for and accepts responsibility for releasing this material on behalf of any and all co-authors. The copyright transfer covers the exclusive right to reproduce and distribute the article, including reprints, translations, photographic reproductions, microform, electronic form (offline, online) or any other reproductions of similar nature.

Authors Contributions

Shuai-ling Lan: Writing original draft, editing and experimental research. Meng Qi: Conceptualization, review. Ming-xian Liu: Experimental research. Wen-bo Bie: Supervision.

References

1. Lu LX, Sun J, Li L et al (2016) Study on surface characteristics of 7050-T7451 aluminum alloy by ultrasonic surface rolling process. Int J Adv Manuf Technol 87(9–12):1–7
2. Zhuang W, Liu Q, Djugum R et al (2014) Deep surface rolling for fatigue life enhancement of laser clad aircraft aluminum alloy. Appl Surf Sci 320(320):558–562
3. Zulan R(2016) Experimental Study on high-cycle fatigue life enhancement of shot-peening Al alloy.Hot Working Technology, :134–136
4. Wang H, Song G, Tang G (2015) Enhanced surface properties of austenitic stainless steel by electro pulsing-assisted ultrasonic surface rolling process. Surf Coat Technol 282(51):149–154
5. Liu Y, Zhao X, Wang D (2014) Effective FE model to predict surface layer characteristics of ultrasonic surface rolling with experimental validation. Mater Sci Technol 30(06):627–636
6. Dai K, Shaw L (2007) Comparison between shot peening and surface Nano-crystallization and hardening process. Mater Sci Eng 463(1–2):46–53
7. Liu Y, Wang LJ, Wang DP (2011) Finite element modeling of ultrasonic surface rolling process. J Mater Process Technol 211(116):2016–2113
8. Chen LQ, Xiang B, Ren XC et al (2014) Influence of surface ultrasonic rolling process parameters on surface condition of axle steel sued on high speed train. China Surf Eng 27(5):1–7
9. Zhu YL, Li L, Wang K et al (2009) An Integrated Ultrasonic Deep Rolling and Burnishing Technology for Anti-fatigue Manufacturing. J Mech Eng 45(9):184–186

10. Bozdana AT, Gindy NNZ (2008) Comparative experimental study on effects of conventional and ultrasonic deep cold rolling processes on Ti-6Al-4V. Mater Sci Technol 24(11):1378–1384
11. Minglong C, Deyuan Z, Huawei C et al (2016) Surface Nano-crystallization and its effect on fatigue performance of high-strength materials treated by ultrasonic rolling process. Int J Adv Manuf Technol 83(1–4):123–131
12. Yang W, Liu P, Xu L et al (2015) Research on fatigue property experiments of 2D12 aluminum alloy by ultrasonic rolling processing. Light Alloy Fabrication Technology 10(12):61–68
13. Zhao YC, Zhang F (2017) Effect of static pressure on surface characteristics of ultrasonic rolling. Surf Technol 46(5):152–158
14. Zhao J, Wang B, Liu ZQ (2016) The investigation into burnishing force, burnishing depth and surface morphology in rotary ultrasonic burnishing. Acta Armamentarium 37(4):696–704
15. Ye H, Lai LS, Li J (2018) el at. Surface properties of 7075 aluminum alloy workpieces after ultrasonic burnishing processing. Surface Technology. 47(2): 8–13
16. Zheng JX, Jiang SX (2017) Residual stress field in the process of 2D ultrasonic rolling 7050 aluminum alloy. Surf Technol 46(12):265–269
17. Ye H, Lai LS, Li J et al (2018) Surface properties of 7075 Aluminum alloy workpieces after ultrasonic burnishing processing. Surf Technol 47(2):8–13
18. Zhao J, Wang B, Liu ZQ (2016) The investigation into burnishing force, burnishing depth and surface morphology in rotary ultrasonic burnishing. Acta Armamentarium 37(4):696–704
19. Zhao YC, Wen CB (2017) Simulation of 3D residual stress field of ultrasonic surface rolling by dynamic finite element analysis. J Mech strength 39(4):875–881
20. Liu Y, Wang L, Wang D (2011) Finite element modeling of ultrasonic surface rolling process. J Mater Process Tech 211(12):2106–2113
21. K. L. Johnson. Contact mechanics [M]. England:The University of Cambridge,
22. Xu HY, Huang YY, Cui FK (2018) A model for surface residual stress of ultrasonic rolling extrusion bearing ring. J Plast Eng 25(05):205–211
23. Research on ultrasonic rolling hardening of gear (2014) Dalian:Dalian University of technology,
24. Li J, Ling X, Zhou J (2012) Finite Element Simulation of Residual Stress Field Induced by Ultrasonic Impact Treatment. J Aeronaut Mater 32(1):84–88

Figures

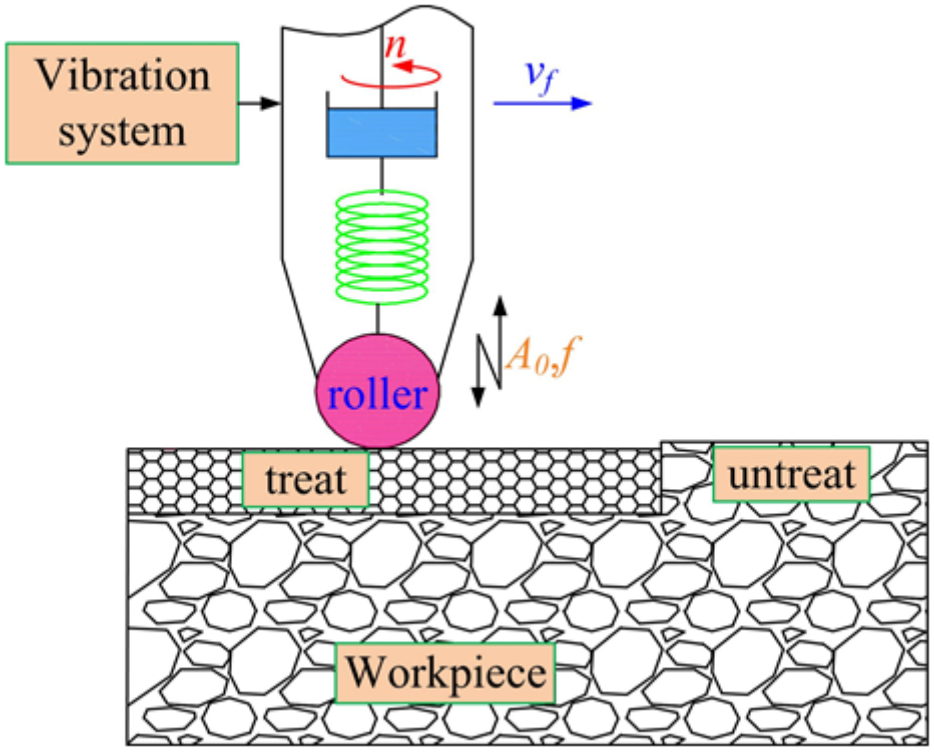

Figure 1

The principle of ultrasonic rolling

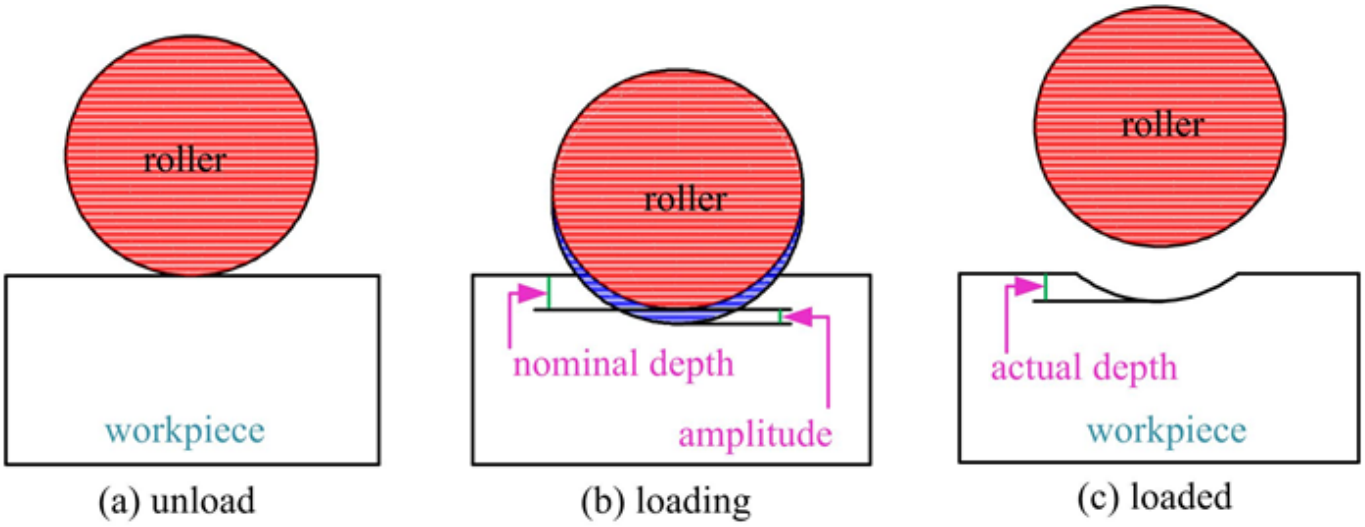

Figure 2

Schematic diagram illustrating the rolling depth of in-plane ultrasonic rolling

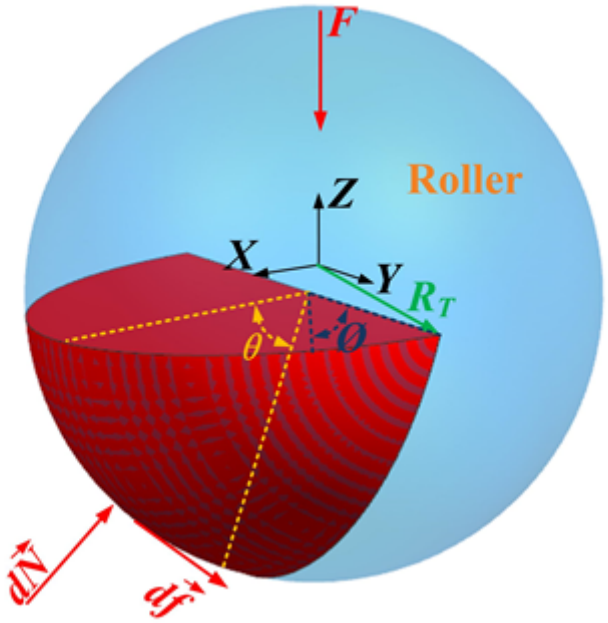

Figure 3

Mechanics of the rolling condition

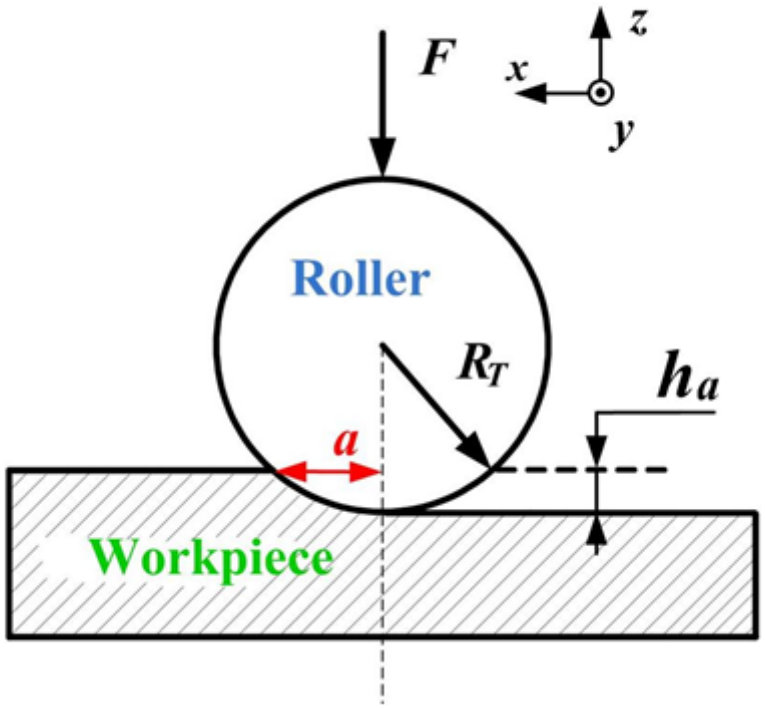

Figure 4

The geometric contact model between the roller and the workpiece

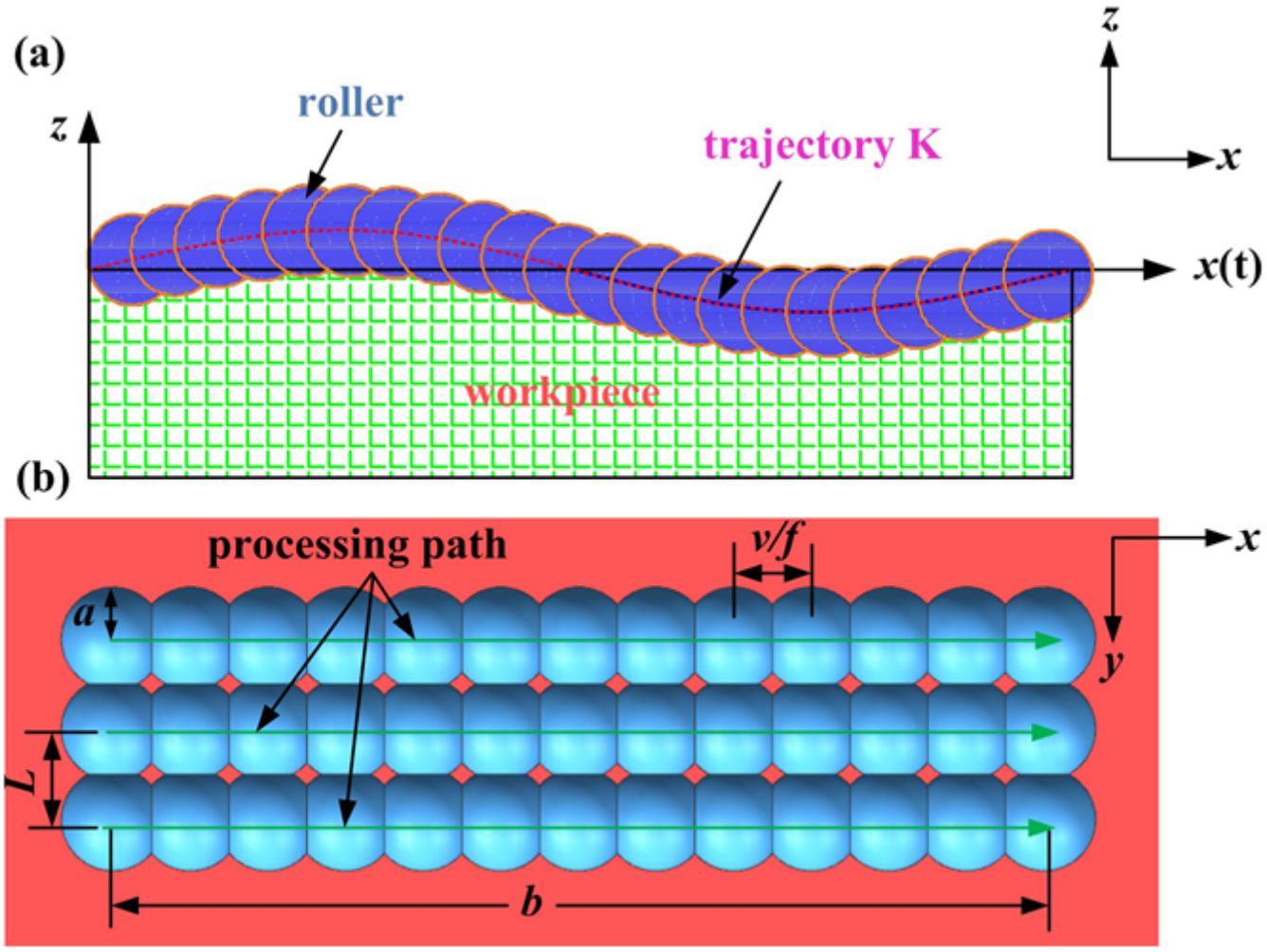

Figure 5

The contact characteristics between the workpiece and the roller

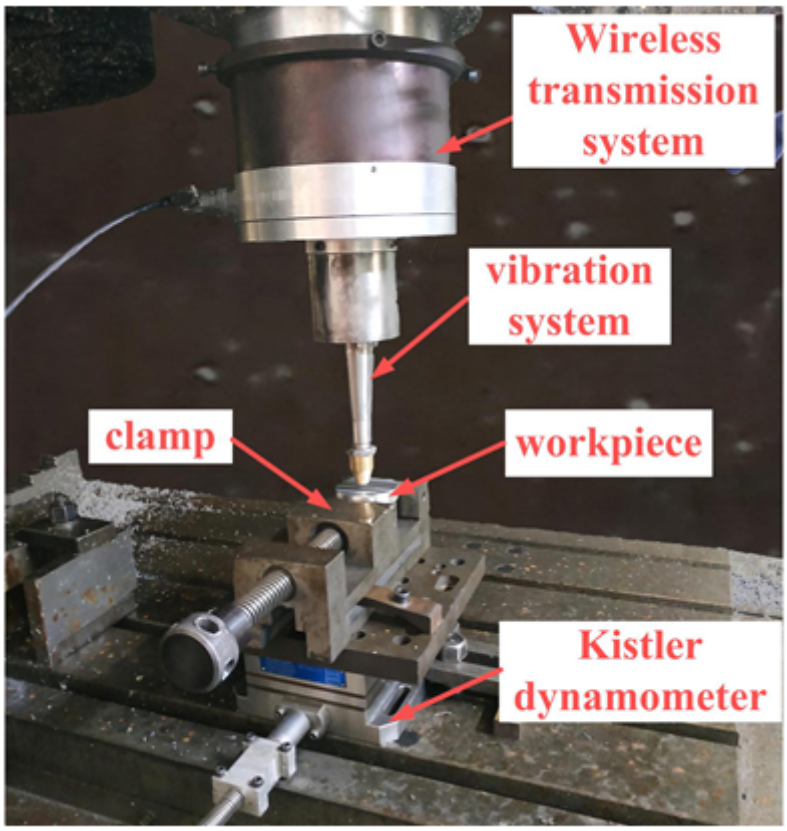

Figure 6

The ultrasonic rolling test apparatus

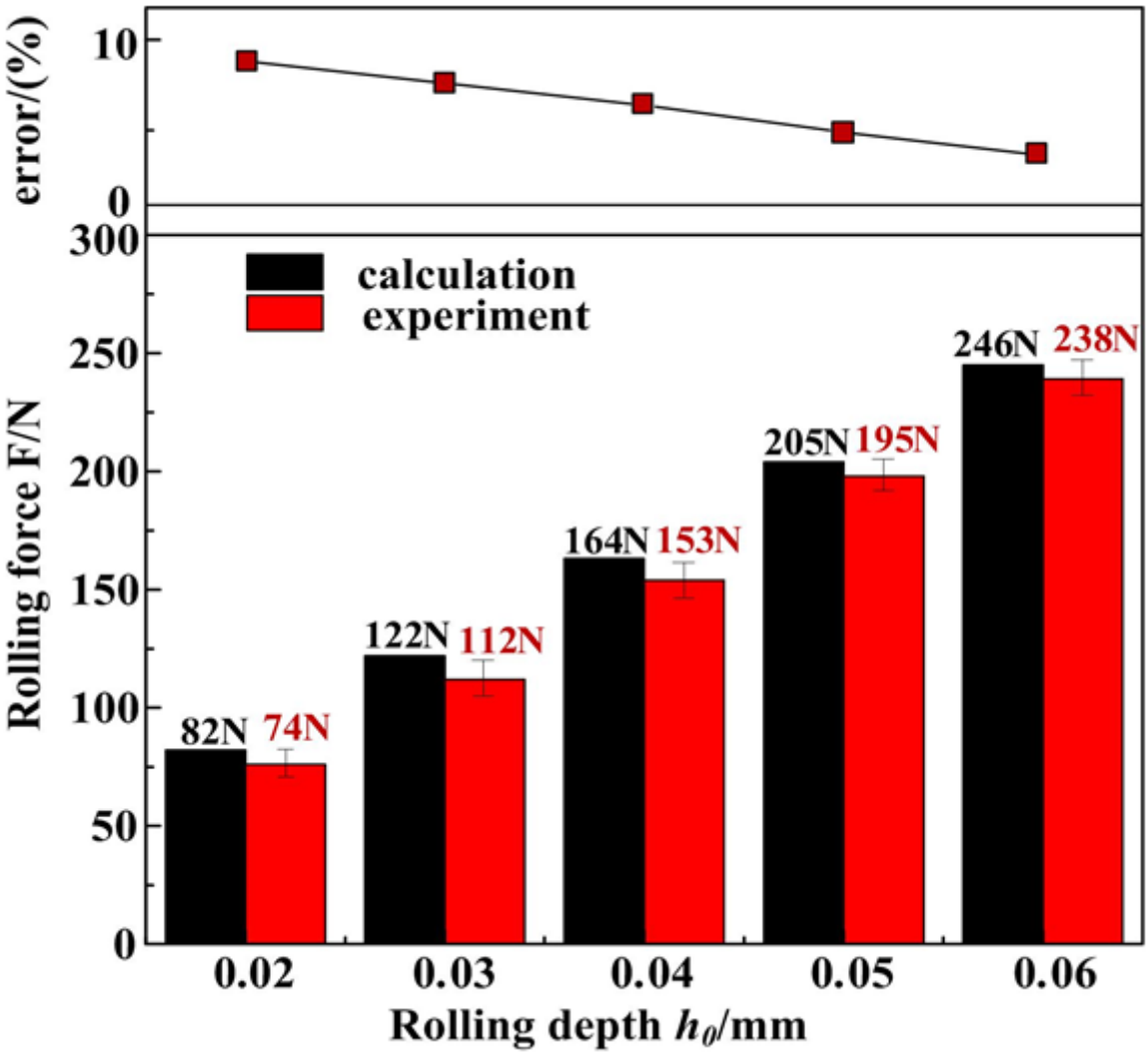

Figure 7

Theoretical values vs. physical test values of the rolling force

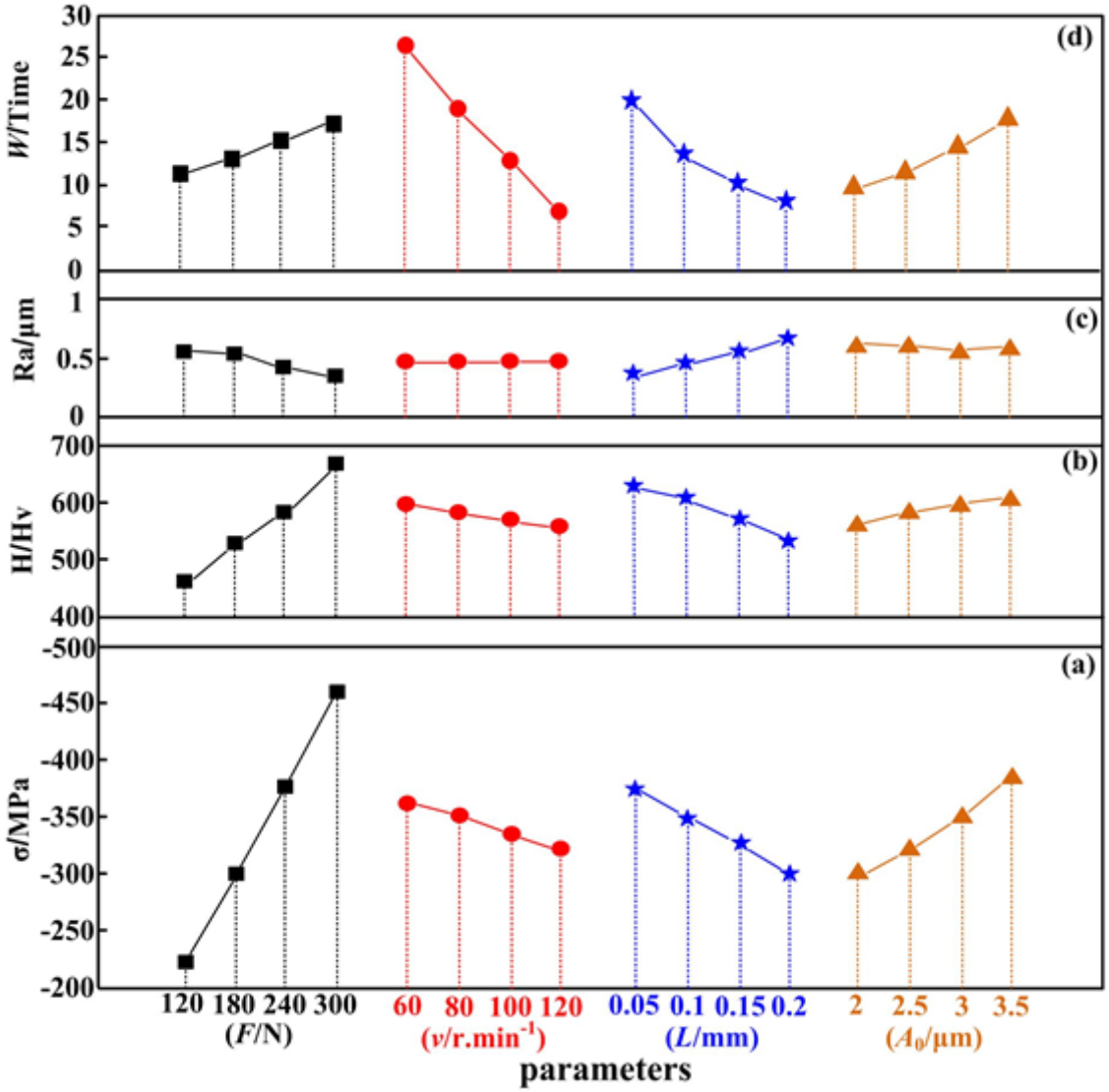

Figure 8

Influence of the parameters on surface properties and the impact characteristics

Figure 9

Influence of impact characteristics on surface morphology

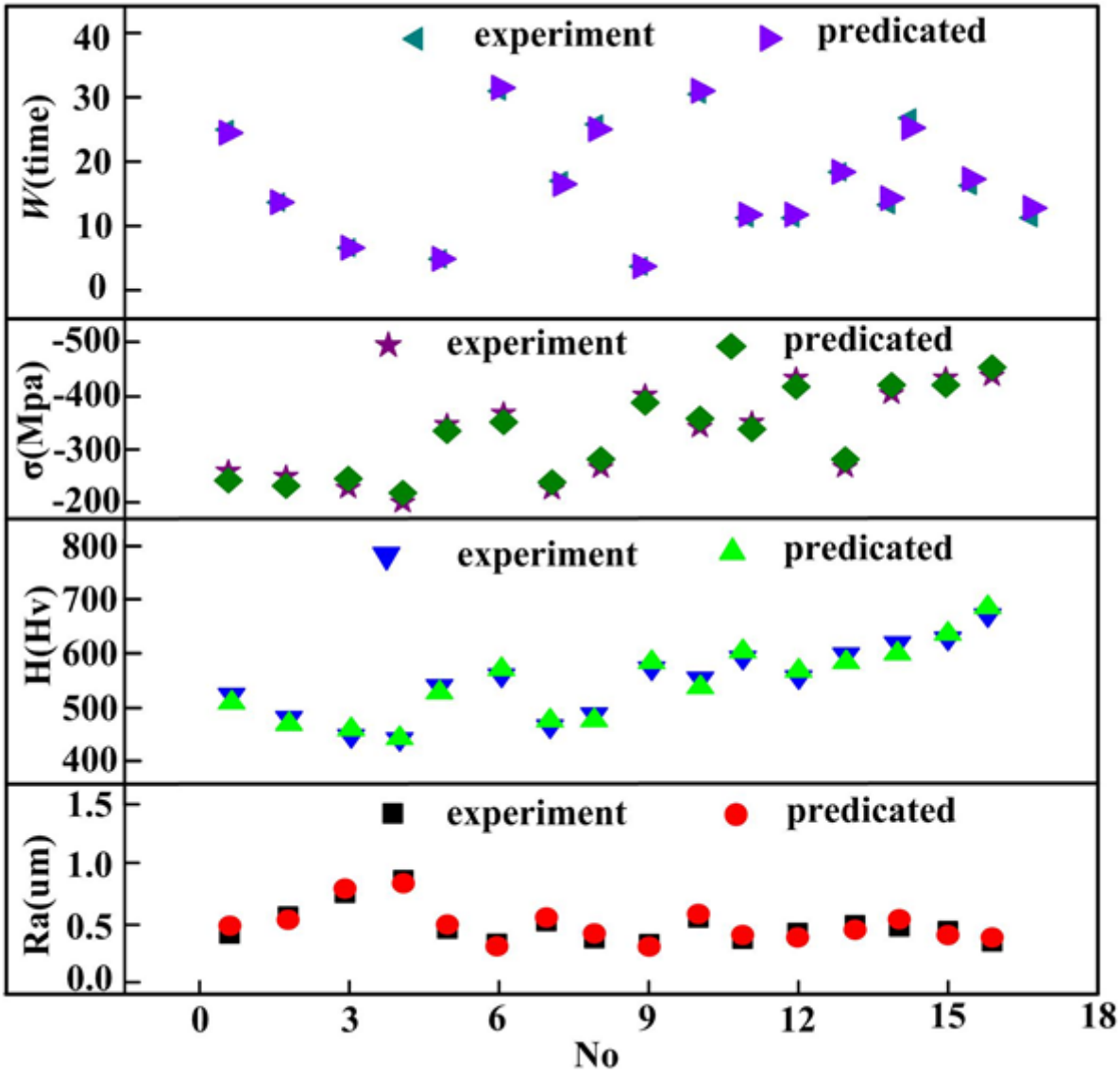

Figure 10

Predicted values vs. physical test data